Systematic investigation on the geometric dependence of the calculated nuclear magnetic shielding constants

ARTICLE *in* JOURNAL OF COMPUTATIONAL CHEMISTRY · AUGUST 2008

Impact Factor: 3.59 · DOI: 10.1002/jcc.20941 · Source: PubMed

3 AUTHORS, INCLUDING:

Igor Ying Zhang
Fritz Haber Institute of the Max Planck Society
34 PUBLICATIONS **746** CITATIONS
SEE PROFILE

Yijing Yan
The Hong Kong University of Science and Tec…
225 PUBLICATIONS **5,414** CITATIONS
SEE PROFILE

Systematic Investigation on the Geometric Dependence of the Calculated Nuclear Magnetic Shielding Constants

YING ZHANG,[1] XIN XU,[1] YIJING YAN[2]
[1]*State Key Laboratory of Physical Chemistry of Solid Surfaces, Center for Theoretical Chemistry, College for Chemistry and Chemical Engineering, Xiamen University, 361005, China*
[2]*Department of Chemistry, Hong Kong University of Science and Technology, Kowloon, Hong Kong*

Received 8 October 2007; Revised 16 December 2007; Accepted 9 January 2008
DOI 10.1002/jcc.20941
Published online 19 March 2008 in Wiley InterScience (www.interscience.wiley.com).

Abstract: We perform a systematic examination on the dependence of the calculated nuclear magnetic shielding constants on the chosen geometry for a selective set of density functional methods of B3LYP, PBE0, and OPBE. We find that the OPBE exchange-correlation functional performs remarkably well when either the optimized geometries or the experimental geometries are used. The popular B3LYP and PBE0 functionals have a clear tendency of deshielding, giving shieldings that are usually too low and shifts that are usually too high, at the experimental geometries. Combined with the Hartree-Fock geometries, however, much improved magnetic constants are obtained for B3LYP and PBE0, due to the compensation effect from the systematic underestimation of bond lengths by the Hartree-Fock method.

 J Comput Chem 29: 1798–1807, 2008

Key words: density functional theory; nuclear magnetic resonance; magnetic shieldings; chemical shifts; geometry; GIAO

Introduction

Nuclear Magnetic Resonance (NMR) spectroscopy continues to be the most valuable tool for structure elucidation.[1] It is well proven that chemical shifts are very valuable in distinguishing differences in electronic environment that arise from chemical reaction, geometric isomerism, hydrogen bonding, adsorption, etc. Dramatic advances in experimental techniques of NMR have much increased the ability to measure chemical shifts, but their interpretation is often based on a heuristically-driven procedure using empirical structural increment rules, which may fail when the sample structure is uniquely different from those in the database. This calls for a decisive, yet efficient, computational method from first principles.

The increasing awareness of this importance has stimulated the development of useful *ab initio* approaches in the calculations of NMR properties in the past few decades.[2–4] It is now well known that valuable information has already been obtained at the level of Hartree-Fock (HF) for simple organic molecules. In the situation where the electronic correlation effects are important, post-HF methods such as the second order Møller-Plesset perturbation method (MP2), the couple cluster method with single and double substitutions plus non-iterative triple excitation (CCSD(T)), and the multi-configuration self-consistent-field method (MC-SCF), etc. have to be adopted.[5–13] These calculations are, however, restricted by their computational time and cost, being impractical for larger chemically interesting molecules.

Recently, methods based on density functional theory (DFT) have become popular.[3,14–23] These methods have a marked accuracy combined with a favorable cost-to-benefit ratio. Thus the last decade has witnessed the great success of DFT in predicting electronic structures, reaction energetics, molecular geometries, etc.[3] In the calculating of the NMR properties, however, the current DFT methods have some unsolved fundamental problems, e.g., the current density dependency is not included,[20] and it is not free from self-interaction error,[18] etc. Hence, Magyarfalvi and Pulay claimed that the commonly used density functionals such as BLYP and B3LYP are significantly inferior to HF for general organic molecules, due to the severe tendency for DFT

This article contains supplementary material available via the Internet at http://www.interscience.wiley.com/jpages/0192-8651/suppmat.

Correspondence to: X. Xu; e-mail: xinxu@xmu.edu.cn

Contract/grant sponsor: National Science Foundation of China; contract/grant numbers: 20525311, 10774126, 20533030, 20423002

Contract/grant sponsor: Ministry of Science and Technology of China; contract/grant numbers: 2004CB719902, 2007CB815206

methods to underestimate the shieldings.[17] Handy and coworkers concluded that the exchange-correlation functionals determined from energy criteria are not optimal for nuclear shielding predictions; and that DFT is not yet competitive with the *ab initio* correlated calculations for the prediction of the NMR shielding constants.[14]

Validation of a theoretical method for its behavior in the NMR calculations is not always straightforward.[1] For one thing, the reference experimental data is affected by intermolecular interactions and intramolecular motion, which, in the gas phase, are observed as the density dependence and the temperature dependence. Even in the zero-pressure limit, the observed nuclear magnetic shielding is a thermal average isotropic shielding that depends on the thermal average of all the internuclear distances in a molecule. One may label the observed NMR shielding as σ_0 and the chemical shift as δ_0, referring to a vibrating and rotating molecule at about 300 K.[1] On the other hand, our calculations of the magnetic properties are generally performed for a single non-vibrating molecule at a fixed geometry. The rovibrational effects are not taken into account at this stage. The geometry used is often the equilibrium geometry, r_e optimized at certain level of theory. One may thus label the calculated shielding as σ_e and the chemical shift as δ_e, referring to a frozen molecule at 0 K. Fundamentally, for the evaluation of the NMR constants, it is essential to differentiate between the experimental σ_0, δ_0 values and the calculated σ_e, δ_e values. Nevertheless, it is not uncommon to make a direct comparison of these two from a pragmatic point of view.[15,16]

There are increasing efforts devoting to the calculations of the NMR properties by using the DFT methods.[14–23] Improvement has been achieved by considering excitation energy corrections,[19] model exchange-correlation potentials[21] and functionals specially optimized for the NMR calculations,[22] etc. Recently, we have investigated the performance for nuclear magnetic constant calculations for a selective set of density functional methods (B3LYP, PBE0, BLYP, PBEPBE, OLYP, and OPBE).[23,24] The results were compared and contrasted to those from the wavefunction-based HF and MP2 methods, as well as the experimental gas phase data (σ_0, δ_0). We found that the OPBE exchange-correlation functional performs remarkably well, being competitive or even better than MP2. Thus we proposed that OPBE is a good GGA (generalized gradient approximation) functional, determined from the energy criteria, for the prediction of the nuclear magnetic constants.[23,24]

In this contribution, we extend our previous work by performing a systematic examination on the dependence of the calculated nuclear magnetic shielding constants on the chosen geometry. We optimize the geometries at the levels of HF, MP2, or B3LYP and also adopt the experimental geometries. We find that the good performance of OPBE stands for all kinds of geometries and when the rovibrational effects are taken into consideration, rendering OPBE a robust method for the calculations of NMR constants. The popular B3LYP and PBE0 functionals suffer from a clear shortcoming of deshielding, giving shieldings that are too low and shifts that are too high. Combined with the HF geometries, however, much improved magnetic constants are obtained for B3LYP and PBE0, due to the compensation effect from the systematic underestimation of bond lengths by the HF method.

Computational Details

We have examined the performance of three functionals B3LYP, PBE0, and OPBE. B3LYP is based on Becke's three parameter scheme.[25] It consists of Slater exchange,[26] the exchange functional of Becke88,[27] and the HF exchange, as well as a mixture of the correlation functionals of Vosco-Wilk-Nusair[28] and Lee-Yang-Par.[29] The contribution of each component to the B3LYP energy expression was fitted empirically on a reference set of molecular energies. B3LYP has distinguished itself as the method of choice for the calculations of a variety of molecular properties. PBE0 was claimed to be a parameter free hybrid functional.[30] Although parameters in the PBE exchange-correlation functional were fixed by the consideration of physical and mathematical constraints,[31] the mix coefficient for the amount of the HF exchange is a predetermined parameter assuming that the fourth-order perturbation theory is sufficient to get accurate numerical results for molecular systems.[32] Specifically, PBE0 was claimed to lead to chemical accuracy for the prediction of NMR shieldings.[16] OPBE is a pure GGA functional. It combines Handy's exchange functional, OPTX,[33] with the correlation functional of PBE.[31] The parameters in OPTX were determined by fitting to the unrestricted HF energies of the first- and second-row atoms. OPTX is unique in that the LDA (local density approximation) limit is lifted. We found that OPBE is the best GGA functional currently available, determined from energy criteria, for the prediction of the nuclear magnetic constants.[23,24]

A set of 23 molecules has been employed as a testing set in the present work.[5–10] For the whole set of molecules, reliable experimental NMR data (σ_0 or δ_0) are available in the gas phase at the zero-pressure limit.[9,15,19,34–38] For some molecules such as (CH_4, H_2O, NH_3, FH, CO, F_2, and N_2), the experimental σ_e, δ_e values are also available.[9,39–45] For some other molecules, we estimate the experimental σ_e, δ_e values by adding the experimental σ_0, δ_0 values with the theoretical rovibrational corrections at the level of MP2[46] or HF.[47,48]

In all our NMR calculations, the gauge including atomic orbital (GIAO) method,[49] as implemented in the Gaussian 03 program suite,[50] was employed. We adopted the 6-311+G(2d,p) basis set as recommended by Cheeseman et al.[15] As for the molecular geometry, we used the optimized ones, obtained at the levels of HF, MP2, and B3LYP using the basis set of either 6-31G(d) or 6-311+G(2d,p). To further examining the geometric dependence of the calculated NMR shieldings and shifts, we also adopted the experimental data at the equilibrium geometry or near equilibrium geometry.[51–62]

Results and Discussion

Geometric Parameters

There are different experimental geometries, e.g., r_e, r_m, r_s, r_0, r_g, etc. (see Refs. [52–54] for definitions), reported in the literature, depending how the structural information is extracted from the experiment results. The best representation, corresponding to the *ab initio* optimized molecular geometry, is the equilibrium structure (r_e). Unfortunately, experimentally determined r_e is only available for a few organic molecules, because it requires either

the determination of the cubic force field or the analysis of, at least, all the fundamentally excited vibrational states for all the required isotopic species. For the set of the 23 molecules used here, we have 17 molecules (N_2,[51,53] F_2,[51,53] CO,[51,53] HF,[51] H_2O,[52] HCN,[51] CO_2,[62] C_2H_2,[51] H_2CO,[51] NH_3,[52] CH_4,[55] CH_3F,[54] CF_4,[58] C_2H_4,[51] CH_3CN,[59] C_3H_4 (allene),[57] C_6H_6[56]) where the experimental r_e have been determined. For other molecules, we have to retreat to r_m (for C_2H_6[54] and C_3H_8 (propane)[54]); r_s (for CH_3OH[60] and CH_3COCH_3[52]); and r_0 (for CHF_3[61] and CH_3NH_2[54]). The inconsistency of the experimental geometries by definition for the whole set may lead to artificial and/or irregular trends, which may hamper a consistent comparison between theory and experiment.

Geometry optimization is now routinely applied in computational chemistry. The equilibrium r_e geometry is obtained by optimization at the various levels of theory. The *ab initio* results may suffer from the uncertainty introduced by the deficiencies in the basis set and the incomplete treatment of the correlation effects. However, this uncertainty may be systematic and the correction factors may be derived empirically so that even modest levels of theory may be used to predict molecular structures with an accuracy, which is competitive with the best experimental methods (i.e., 0.003 Å and 0.5°).[63]

The G2 method developed by Curtiss et al. is a composite method for highly accurate prediction of molecular energies.[64] The geometry used in G2 is based on the optimization results using the second-order Møller–Plesset (MP2) perturbation theory combined with the 6-31G(d) basis set. Later, it was found that the replacement of the MP2/6-31G(d) geometry and the scaled zero-point energy at the HF/6-31G(d) level with the corresponding B3LYP/6-31G(d) value not only enhanced the efficiency, but also increased the accuracy.[65] Further investigations showed that B3LYP combined with the basis set of triple-zeta quality (e.g., 6-311G(d,p)[30]) provides nearly converged structural parameters. Therefore, we optimize the molecular geometries at the levels of HF, MP2 and B3LYP by using basis sets of either 6-31G(d) or 6-311+G(2d,p) The results may be found in the supplementary material (Tables S1 and S2). We denoted the double-zeta basis set as S whereas the triple-zeta basis set as *L*. The statistic data, mean absolute deviations (MADs), as compared to the corresponding experimental values are summarized in Table 1.

It has long been recognized that HF frequently gives bond lengths that are too short, whereas MP2 tends to overestimate the correlation effects, leading to bond lengths that are usually too long.[66] This general tendency is faithfully reproduced by our calculations. Thus our calculations give mean deviations, (theo.–exp.), of −0.0109 and +0.0042 Å for HF and MP2, respectively, at the S basis set. For HF/S, the largest negative deviations in bond length, (theo.–exp.) < −0.02 Å, occur at C—H, F—F, C—N, and C—O bonds in CH_3F, F_2, HCN, CH_3CN, CH_3OH, and CH_3COCH_3, whereas for MP2/S, the largest positive deviations in bond length, (theo.–exp.) > +0.02 Å, occur at N—N, C—N, and C—O multiple bonds in N_2, HCN, CH_3CN, and CO (see Table S1). Increasing basis set always leads to a contraction of the bond length. Hence the agreement with experiment is enhanced with the increase of the basis set from S to L for the MP2 method, whereas the reverse is observed for the HF method. The mean deviations for HF/L and MP2/L are −0.0140 and +0.0025 Å, respectively.

Table 1 demonstrates that B3LYP/S is superior to MP2/S for the geometry predictions. While the accuracy is slightly worse for the 25 comparisons of the X—H bonds, B3LYP/S is significantly better than MP2/S for the 21 comparisons of the X—Y bonds (X,Y ≠ H). When going from MP2/S to B3LYP/S, MAD for the CC single, double and triple bonds decreases by 5%. Interestingly, MAD further decreases dramatically by another 27% when the difficult cases such as N_2 and F_2 for *ab initio* methods are included for comparison. For bonds between non-

Table 1. Mean Absolute Deviations (MADs) of Theoretical Structures from Experimental Values.[51–62]

Structural type	Number of comparisons	Mean absolute deviations (MADs)					
		HF/S	HF/L	MP2/S	MP2/L	B3LYP/S	B3LYP/L
CH	20	0.0065	0.0069	0.0054	0.0036	0.0071	0.0042
XH (X≠C)[a]	5	0.0113	0.0164	0.0086	0.0032	0.0092	0.0044
CC[b]	8	0.0105	0.0108	0.0055	0.0032	0.0052	0.0060
XX[c]	10	0.0170	0.0199	0.0085	0.0043	0.0058	0.0066
XY (X≠Y)[d]	11	0.0189	0.0243	0.0210	0.0079	0.0072	0.0065
Bond lengths	**46**	0.0123	0.0149	0.0101	0.0048	0.0070	0.0053
HCH	11	0.52	0.39	0.60	0.39	0.69	0.46
HXH[e]	14	0.60	0.63	0.53	0.44	0.72	0.52
Other angles[f]	9	0.53	0.65	0.33	0.28	0.42	0.43
Bond angles	**23**	0.57	0.64	0.45	0.38	0.60	0.48

Bond distances in angstroms, bond angles in degrees.
[a]NH, OH, and FH single bonds.
[b]CC single, double, and triple bonds.
[c]CC single, double, and triple bonds, plus NN triple bond and FF single bond.
[d]CN triple bonds, CF single bonds, and CO single and double bonds.
[e]HCH, plus HNH, and HOH angles.
[f]HCC, HCN, HCO, OCC, and FCF angles.

Table 2. Mean Absolute Deviations (MADs) of the Theoretical Magnetic Shieldings from the Experimental Values (σ_0).[9,15,19,34–38]

Methods		MAD (^{13}C)	MAD (^{15}N, ^{17}O,^{19}F)	MAD (tot)	Maximum error
HF/S opt. geom.	B3LYP	5.65	**18.74**	10.27	162.82 (F_2)
	PBE0	**1.99**	19.09	**8.02**	173.75 (F_2)
	OPBE	4.52	21.39	10.48	165.23 (F_2)
HF/L opt. geom.	B3LYP	4.67	**23.34**	11.26	197.52 (F_2)
	PBE0	**1.72**	23.42	**9.38**	208.21 (F_2)
	OPBE	5.35	26.45	12.79	200.39 (F_2)
MP2/S opt. geom.	B3LYP	11.59	20.78	14.83	−49.59 (N_2)
	PBE0	6.62	19.15	11.04	−48.06 (N_2)
	OPBE	**2.24**	**17.07**	**7.48**	−46.32 (F_2)
MP2/L opt. geom.	B3LYP	10.24	12.88	11.17	−34.24 (N_2)
	PBE0	5.33	11.84	7.62	−32.79 (N_2)
	OPBE	**1.86**	**9.87**	**4.69**	−23.14 (HC*N*)
B3LYP/S opt. geom.	B3LYP	10.14	14.28	11.60	−26.78 (N_2)
	PBE0	5.20	12.61	7.81	−25.37 (N_2)
	OPBE	**2.30**	**7.50**	**4.14**	−24.16 (CHF_3)
B3LYP/L opt. geom.	B3LYP	8.77	10.84	9.50	−20.43 (CHF_3)
	PBE0	3.88	9.64	5.91	29.11 (F_2)
	OPBE	**2.80**	**7.71**	**4.53**	−23.81 (CHF_3)
B3LYP/L exp. geom.	B3LYP	8.97	11.76	9.95	−21.08 (CH_3CN)
	PBE0	4.19	8.85	5.83	−18.65 (N_2)
	OPBE	**2.19**	**6.97**	**3.88**	−18.97 (CHF_3)

The maximum positive or negative error (theo.–exp.) for each method is also included. Numbers in bold faces represent the best method in each entry.

hydrogen heteroatoms (X—Y), the situation is also much improved for B3LYP/S. While MAD of MP2/S is as high as 0.021 Å, it decreases dramatically to 0.007 Å for B3LYP/S.

Increasing the basis set generally decreases the errors for geometry predictions for B3LYP. We notice that there are many cases where the bond lengths that are too long for B3LYP/S, but too short for B3LYP/L. This trend shows up for N—N in N_2; C—O in CO, CO_2, H_2CO, and CH_3OH; C—N in HCN and CH_3CN; C—C in C_2H_2 and C_6H_6; C—H in CH_3F, CH_3NH_2, and CH_3OH, C_6H_6, etc. (see Table S1).

We have also examined 23 bond angles (see Table S2). The deviation from the experiment is all around 0.5°. HF/S leads to bond angles that are too large, whereas MP2/S and B3LYP/S give bond angles that are usually too small. Thus our calculations give mean deviations, (theo.–exp.), of +0.14, −0.14, and −0.27°, respectively. Increasing basis set tends to increase the bond angles. Hence the calculated mean deviations are +0.39, +0.17, +0.14, indicating the calculated bond angles are statistically too large at the L basis set. HF is poor for the description of the HOH, COH, and CNH bond angles due to the improper treatment of the interaction between lone-pair electrons and bonding electrons, demonstrating the importance of the electron correlation effect. All in all, B3LYP is worse than MP2 for the description of bond angles.

Based on the MADs in Table 1, we may conclude that the accuracy for the geometry prediction follows the order that MP2/L > B3LYP/L > B3LYP/S > MP2/S > HF/S > HF/L. The general trend is that increasing the basis set tends to decrease the bond lengths and increase the bond angles. Because of the fundamental shortcoming of the approximation made in the theory, large basis set calculations may overshoot the experimental values, giving results that are even worse than those from the small basis set calculations.

As NMR shielding constants are very sensitive to the geometric change, we will see that small differences in the geometry can have large effects on the calculated magnetic constants.

Magnetic Shieldings

Tables 2 and 3 summarize MADs for the calculated magnetic shieldings, with respect to the experimental σ_0 and σ_e, respectively, using geometries optimized with *ab initio* methods of HF/S, HF/L, MP2/S, and MP2/L. The maximum positive or negative error, (theo.–exp.), for each method is also included. Numbers in bold faces represent the best method in each entry. This set of molecules includes 22 comparisons for carbon nucleus, 4 for fluorine, 3 for oxygen, and 5 for nitrogen in various environments (see Table S3).

Taking the experimental gas phase data σ_0 as reference and calculating the magnetic shieldings at the experimental geometries, we find that OPBE leads to MADs of 2.19 for ^{13}C, and 6.97 for ^{15}N, ^{17}O, and ^{19}F, giving a total MAD = 3.88 ppm for the whole set. In comparison, PBE0 leads to MADs of 4.19 (^{13}C), 8.85 (^{15}N, ^{17}O, and ^{19}F), and 5.83 ppm (tot), whereas B3LYP leads to MADs of 8.97 (^{13}C), 11.76 (^{15}N, ^{17}O, and ^{19}F), and 9.95 ppm (tot). Clearly, the most popular B3LYP is least useful for the shielding calculations. It is seen (from Table S3) that B3LYP has a severe tendency of underestimating the shieldings.[14,17] For a total of 34 comparisons examined here, there are only two cases, +3.07 ppm for ^{17}O in H_2O and +1.68 for ^{19}F in

Table 3. Mean Absolute Deviations (MADs) of the Theoretical Magnetic Shieldings from the Experimental Values (σ_e).[9,39–48]

Methods		MAD (^{13}C)	MAD (^{15}N, ^{17}O, ^{19}F)	MAD (tot)	Maximum error
HF/S opt. geom.	B3LYP	8.35	17.69	11.65	122.82 (F_2)
	PBE0	3.67	**16.45**	**8.18**	133.75 (F_2)
	OPBE	**3.12**	18.83	8.66	125.23 (F_2)
HF/L opt. geom.	B3LYP	7.37	20.36	11.95	157.52 (F_2)
	PBE0	**2.97**	**18.83**	**8.57**	168.21 (F_2)
	OPBE	3.77	22.57	10.40	160.39 (F_2)
MP2/S opt. geom.	B3LYP	14.29	29.56	19.68	−84.50 (F_2)
	PBE0	9.33	27.92	15.89	−72.81 (F_2)
	OPBE	**3.86**	**25.85**	**11.62**	86.32 (F_2)
MP2/L opt. geom.	B3LYP	12.94	21.65	16.02	−51.40 (F_2)
	PBE0	8.03	19.99	12.25	−39.75 (F_2)
	OPBE	**2.98**	**18.29**	**8.38**	−52.38 (F_2)
B3LYP/S opt. geom.	B3LYP	12.84	21.78	15.99	−32.35 (F_2)
	PBE0	7.90	18.18	11.53	−27.37 (N_2)
	OPBE	**3.17**	**15.08**	**7.37**	−32.87 (F_2)
B3LYP/L opt. geom.	B3LYP	11.47	16.70	13.32	−28.43 (CHF_3)
	PBE0	6.58	13.18	8.91	−23.09 (CHF_3)
	OPBE	**3.31**	**11.98**	**6.37**	−31.81 (CHF_3)
B3LYP/L exp geom.	B3LYP	11.67	19.74	14.52	−57.26 (F_2)
	PBE0	6.80	16.26	10.14	−45.61 (F_2)
	OPBE	**2.85**	**13.56**	**6.63**	−58.39 (F_2)

The maximum positive or negative error (theo. – exp.) for each method is also included. Numbers in bold faces represent the best method in each entry.

HF, where deviations (theo.–exp.) are positive; all others are negative. Specifically, for ^{15}N in N_2, HCN and CH_3CN, the deviations are as large as −20 ppm, leading to the net signed deviations of −8.97 (^{13}C), −7.65 (^{15}N, ^{17}O, and ^{19}F), and −8.51 ppm (tot) for B3LYP.

PBE0 also shows a tendency of deshielding, although in a less degree as compared to B3LYP. Among the 34 comparisons (see Table S3), there are only 4 cases where the deviations from the experiments are positive. These are +0.33 for $CH_3CH_2CH_3$, +0.57 for CH_3COCH_3, +5.04 for H_2O, and +3.16 ppm for H*F*. The biggest negative deviations also occur at the nitrogen nucleus of N_2, HCN and CH_3CN. They are all around −18 ppm. The net signed deviations for PBE0 are −4.10 (^{13}C), −6.09 (^{15}N, ^{17}O, and ^{19}F) and −4.81 ppm (tot).

OPBE differs from B3LYP and PBE0, statistically showing a tendency of overshielding (see Table S3). Among the 34 comparisons, there are 22 cases with positive deviations and 10 cases with negative deviations. For the difficult cases of ^{15}N, OPBE gives deviations of only +0.89 (N_2), +1.38 (HCN), and −1.90 ppm (CH_3CN). The net signed deviations for OPBE are +1.71 (^{13}C), −0.26 (^{15}N, ^{17}O, and ^{19}F), and +1.02 ppm (tot), significantly outperforming B3LYP and PBE0. On the other hand, OPBE suffers from its own shortcoming for the description of ^{19}F, leading to deviations of −18.39 (F_2), −16.13 (CH_3F), and −18.97 ppm (CHF_3). For shieldings of fluorine nucleus, the best performer is PBE0, giving −5.61 (F_2), −3.69 (CH_3F), and −10.53 ppm (CHF_3). B3LYP is in between OPBE and PBE0, giving −17.26 (F_2), −8.73 (CH_3F), and −15.75 ppm (CHF_3). The signed deviations for each molecule calculated with B3LYP, PBE0 and OPBE at the experimental geometries are depicted in Figure 1.

As it is nontrivial to deduce the r_e geometry purely by means of experiments,[52,54,56,63] we here examine how the calculated magnetic shieldings be affected by the optimized geometries. This will not only help us to find out a practical method with a favorable cost-to-benefit ratio, but also deepen our understanding on the advantages and limitations of a method. Take the B3LYP/S and B3LYP/L geometries as examples, B3LYP/S tends to overestimate the bond length, this will exacerbate the deshielding effect of B3LYP and PBE0 for the prediction of magnetic shieldings. Increasing the basis set compresses the optimized bond length, which mitigates the deshielding effect. Thus it is seen that from the B3LYP/S geometry to the B3LYP/L geometry, MADs decrease by ∼2 ppm for B3LYP and PBE0, whereas the general performance of OPBE remains stable as statistically overshielding and deshielding effects are counterbalanced for OPBE.

Geometry may have a profound effect on the calculated NMR shieldings. For example, as the N—N bond length in N_2 decreases by 0.0365 Å from B3LYP/S to B3LYP/L, an improvement of ∼12 ppm on the calculated shieldings is observed for B3LYP and OPBE. For different nucleus, the geometric effect may be different. Hence as the C—O bond is decreased by 0.0122 Å, we see that the calculated oxygen shielding is improved by ∼12 ppm, whereas the corresponding carbon shielding is improved by ∼6 ppm for B3LYP and PBE0. As is pointed out in the previous section, for both N—N in N_2 and C—O in CO, the B3LYP/S geometry is too long, whereas the

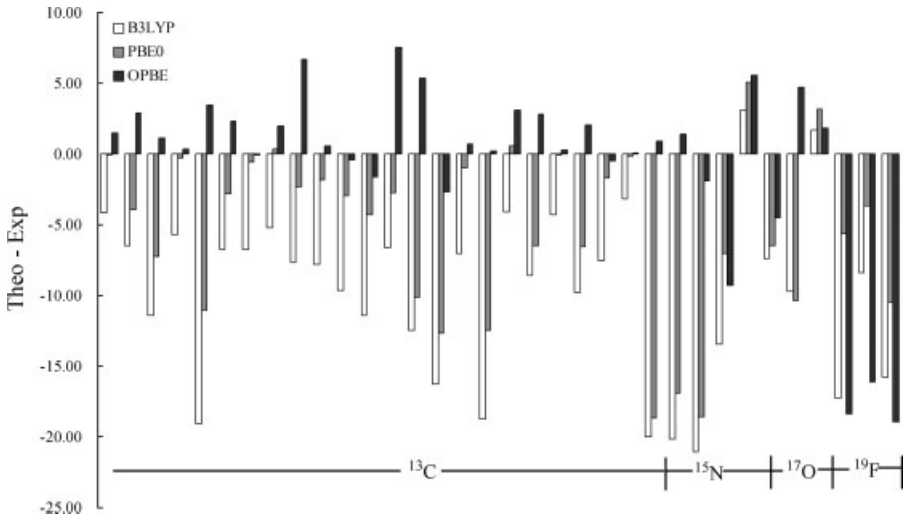

Figure 1. Deviations, (theo.–exp.), with respect to the experimental σ_0 at the experimental geometries.

B3LYP/L geometry is too short as compared to the experimental r_e. F_2, however, represent an extreme case, where the B3LYP/S geometry is already too short by 0.0084 Å. Increasing the basis set leads to the B3LYP/L geometry to decrease by another 0.0034 Å. This makes B3LYP and PBE0 overshoot the experimental σ_0.

Table 2 clearly demonstrates that when B3LYP and PBE0 are combined with the HF geometry for the prediction of magnetic shieldings, the compensation effect takes the most effect. For ^{13}C, MADs decrease from 8.97 (B3LYP) and 4.19 (PBE0) at the experimental geometries to 5.65/4.67 (B3LYP) and 1.99/1.72 (PBE0) at the HF geometries using the S/L basis sets. However, caution must be taken when using the HF geometry. When the correlation effects are important, the HF geometry can be in serious errors. F_2 is a pathologic case in the HF theory.[23] As compared to the experimental geometry, HF/S is too short by 0.067 Å while HF/L is too short by 0.082 Å. These lead to the calculated fluorine nucleus being overshielded up to 162.82/197.52 ppm for B3LYP at the S/L basis sets while the PBE0 calculated fluorine nucleus are overshielded up to 197.52/208.21 ppm at the S/L basis sets. If F_2 is excluded, B3LYP gives MADs = 5.64/7.51 ppm for ^{15}N, ^{17}O, and ^{19}F at the S/L basis sets, whereas the corresponding values for PBE0 are 5.03/6.62 ppm.

In principle, we should compare the calculated shieldings with the experimental σ_e values.[1] Since the rovibration correction ($\sigma_e - \sigma_0$) is systematically positive, we always have $\sigma_e > \sigma_0$ for the experimental values.[1,46–48] Thus if the experimental σ_e is taken as the reference, DFT results should appear even more deshielded (see Table 3). At the experimental geometry and with respect to the experimental σ_e, OPBE leads to MADs of 2.85 for ^{13}C, and 13.56 for ^{15}N, ^{17}O, and ^{19}F, giving a total MAD = 6.63 ppm for the whole set, and being the best method examined here. PBE0 leads to MADs of 6.80 (^{13}C), 16.26 (^{15}N, ^{17}O, and ^{19}F), and 10.14 ppm (tot), whereas B3LYP leads to MADs of 11.67 (^{13}C), 19.74 (^{15}N, ^{17}O, and ^{19}F), and 14.52 ppm (tot). In comparison to MADs with respect to the experimental σ_0, we have an increase of MADs of 0.66 (OPBE), 2.61 (PBE0), and 2.70 ppm (B3LYP) for ^{13}C; and an increase of MADs of 6.59 (OPBE), 7.41 (PBE0), and 7.98 ppm (B3LYP) for ^{15}N, ^{17}O, and ^{19}F. Hence rovibration effect is generally mild for ^{13}C, but can be very strong for ^{15}N, ^{17}O, and ^{19}F. In fact, for F_2 the observed rovibration correction is as large as 40.0 ppm.[45] For oxygen in H_2O and nitrogen in NH_3, the observed rovibration corrections are 13.6[40] and 8.8 ppm,[41] respectively.

It is noteworthy to recall the performance of MP2.[5,23] MP2 tends to overshield, leading to MADs of 10.02 (^{13}C), 23.13 (^{15}N, ^{17}O, and ^{19}F), and 14.60 ppm (tot) with respect to the experimental σ_0.[23] The corresponding MADs with respect to the experimental σ_e are 7.32 (^{13}C), 14.34 (^{15}N, ^{17}O, and ^{19}F), and 9.80 ppm (tot). As it can be anticipated, compensation effect will take effect to reduce MADs, when the shielding prediction is performed at the MP2 level by using the MP2/S geometry. Overshielding effects will deteriorate the results if the HF geometry is adopted.

Chemical Shifts

Chemical shifts for the ^{13}C, ^{15}N, ^{17}O, and ^{19}F nucleus are given relative to gaseous CH_4, NH_3, H_2O, and HF respectively (see Table S4). The statistic data, MADs, at various geometries with respect to the experimental δ_0 and δ_e are summarized in Tables 4 and 5, respectively. The signed deviations, (theo.–exp.), at the experimental geometry with respect to the experimental δ_0 are depicted in Figure 2.

There are several factors that influence the accuracy of the calculated chemical shifts. Specifically, if the error in the calculated magnetic shielding for a given nuclear is similar to that of the reference nuclear in magnitude and the error signs of both are in the same direction, errors are systematic and error cancellations take place. High accuracy in the prediction of chemical shifts can be achieved in this way. MP2 offers such an example. For ^{13}C, MP2 leads to MAD = 10.02 ppm for shieldings, but only 2.68 ppm for shifts,[23] thanks to the systematic overshield-

Table 4. Mean Absolute Deviations (MADs) of the Theoretical Chemical Shifts from the Experimental Values (δ_0).[9,15,19,34–38]

Methods		MAD (^{13}C)	MAD (^{15}N, ^{17}O, ^{19}F)	MAD (tot)	Maximum error
HF/S opt. geom.	B3LYP	2.36	**23.55**	**8.72**	−158.41 (F_2)
	PBE0	**2.12**	24.37	8.80	−167.95 (F_2)
	OPBE	2.94	25.29	9.65	−160.69 (F_2)
HF/L opt. geom.	B3LYP	1.98	27.51	9.64	−188.10 (F_2)
	PBE0	**1.70**	**26.36**	**9.10**	−197.56 (F_2)
	OPBE	3.62	30.76	11.76	−190.84 (F_2)
MP2/S opt. geom.	B3LYP	6.74	20.79	10.96	44.29 (N_2)
	PBE0	5.91	22.03	10.75	45.89 (N_2)
	OPBE	**2.39**	**18.50**	**7.22**	39.97 (F_2)
MP2/Lopt. geom.	B3LYP	5.73	14.53	8.37	29.70 (N_2)
	PBE0	4.93	15.36	8.06	31.32 (N_2)
	OPBE	**1.82**	**12.44**	**5.01**	21.93 (HC*N*)
B3LYP/S opt. geom.	B3LYP	4.43	13.17	7.05	20.73 (N_2)
	PBE0	3.73	14.14	6.85	−23.91 (F_2)
	OPBE	**2.46**	**7.37**	**3.93**	17.89 (CHF_3)
B3LYP/L opt. geom.	B3LYP	3.92	11.10	6.07	−19.29 (F_2)
	PBE0	3.23	11.91	5.84	−29.29 (F_2)
	OPBE	**2.79**	**9.93**	**4.93**	22.17 (CHF_3)
B3LYP/L exp geom.	B3LYP	5.06	14.62	7.93	18.95 (F_2)
	PBE0	4.34	12.97	6.93	18.53 (N_2)
	OPBE	**1.99**	**9.23**	**4.16**	20.78 (CHF_3)

The maximum positive or negative error (theo. – exp.) for each method is also included. Numbers in bold faces represent the best method in each entry.

ing effect associated with MP2. At the experimental geometry and with respect to the experimental δ_0, OPBE, PBE0 and B3LYP lead to MADs of 1.99, 4.34, and 5.06 ppm, respectively, for ^{13}C. While OPBE remains to be the best method, we see that B3LYP takes the full advantage of the error cancellation in predicting chemical shifts, as B3LYP is systematically deshield-

Table 5. Mean Absolute Deviations (MADs) of the Theoretical Chemical Shifts from the Experimental Values (δ_e).[9,39–48]

Methods		MAD (^{13}C)	MAD (^{15}N, ^{17}O, ^{19}F)	MAD (tot)	Maximum error
HF/S opt. geom.	B3LYP	2.44	20.37	7.82	−128.11 (F_2)
	PBE0	**2.06**	**18.01**	**6.84**	−137.65 (F_2)
	OPBE	3.77	23.74	9.76	−130.39 (F_2)
HF/L opt. geom.	B3LYP	2.62	26.49	9.78	−157.80 (F_2)
	PBE0	**2.08**	**23.77**	**8.58**	−167.26 (F_2)
	OPBE	4.51	29.95	12.14	−160.54 (F_2)
MP2/S opt. geom.	B3LYP	6.24	20.17	10.42	68.34 (F_2)
	PBE0	5.43	20.51	9.95	58.37 (F_2)
	OPBE	**2.50**	**16.49**	**6.69**	70.27 (F_2)
MP2/L opt. geom.	B3LYP	5.25	14.46	8.01	40.99 (F_2)
	PBE0	4.47	13.36	7.14	30.89 (F_2)
	OPBE	**2.29**	**11.52**	**5.06**	42.09 (F_2)
B3LYP/S opt. geom.	B3LYP	4.05	8.27	5.32	16.27 (F_2)
	PBE0	3.31	**7.35**	**4.52**	15.72 (N_2)
	OPBE	**3.00**	8.63	4.69	16.90 (F_2)
B3LYP/L opt. geom.	B3LYP	3.72	6.17	4.45	16.97 (CHF_3)
	PBE0	**2.93**	**4.13**	**3.29**	13.21 (CHF_3)
	OPBE	3.40	12.03	5.99	20.47 (CHF_3)
B3LYP/L exp geom.	B3LYP	4.74	12.81	7.16	49.25 (F_2)
	PBE0	3.99	**10.96**	6.08	39.06 (F_2)
	OPBE	**2.62**	13.97	**6.02**	50.50 (F_2)

The maximum positive or negative error (theo. – exp.) for each method is also included. Numbers in bold faces represent the best method in each entry.

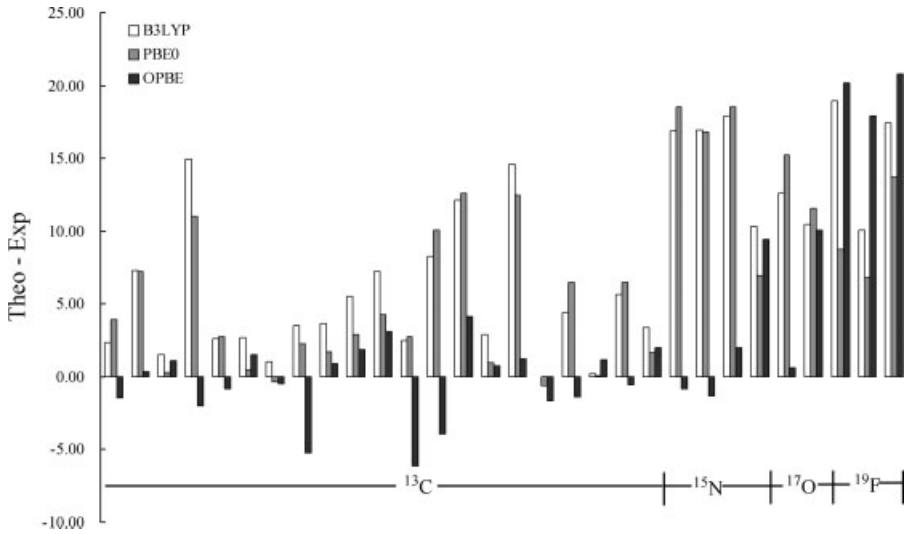

Figure 2. Deviations, (theo.–exp.), with respect to the experimental δ_0 at the experimental geometries.

ing. From shielding to shift, MAD is reduced by 3.91 ppm, which is in parallel with the error (4.14 ppm) in the prediction of shielding of the reference CH_4 molecule by B3LYP.

At the experimental geometry and with respect to the experimental δ_0, OPBE, PBE0 and B3LYP lead to MADs of 9.23, 12.97, and 14.62 ppm, respectively, for ^{15}N, ^{17}O, and ^{19}F. In comparison with the accuracy of the shielding prediction, MADs increase for all methods. One reason for this behavior lies in that all three DFT methods perform less satisfactorily in the description of the given nucleus than of the reference nuclear. For example, B3LYP and PBE0 give absolute deviations of 3.15 and 0.12 ppm for ^{15}N in the reference NH_3 molecule, whereas the absolute deviations are as high as 20.12 (B3LYP) and 16.89 (PBE0) ppm for ^{15}N HCN. For ^{17}O and ^{19}F, another factor makes important contribution to the observed increase of MADs. DFTs lead to errors of different signs for the reference nucleus and the sample nucleus. For example, B3LYP, PBE0 and OPBE are all overshielding for the reference H*F* molecule, giving errors (theo.–exp.) in the calculated shieldings of +1.68, +3.16 and +1.81 ppm. For CHF_3, there is a severe tendency of deshielding, giving errors of −15.75, −10.53, and −18.97 ppm, respectively. These errors in shieldings add up to the errors in shifts, giving absolute errors of 7.43, 13.68, and 20.78 ppm, respectively.

Although Tables 4 and 5 show that OPBE performs remarkably well at the experimental geometry with respect to either the experimental δ_0 or δ_e, this good performance stands when the optimized geometries are used. However, OPBE is much degraded for the description of the fluorine nucleus, leaving room for further improvement.

With respect to the experimental δ_e, PBE0 leads to the smallest MADs at the B3LYP/L geometry. For ^{13}C, MAD is 2.93 ppm; while for ^{15}N, ^{17}O, and ^{19}F, MAD is 4.13 ppm. The geometry effect is stronger for the later than for the former. If the geometries are optimized at the PBE0/L level, MADs are 2.43 ppm for ^{13}C, but 10.06 ppm for ^{15}N, ^{17}O, and ^{19}F,[23] since B3LYP/L gives the F—F distance of 1.4001 Å, whereas PBE0 leads to 1.3787 Å,[23] which significantly diverges from the experimental r_e of 1.4119 Å.[53]

Once again, we see that when combined with the HF geometries, B3LYP and PBE0 lead to good accuracy in the prediction of chemical shifts. Thus B3LYP/PBE0 at the HF/S geometries lead to MADs of 2.36/2.12 (^{13}C), 6.69/6.42 (^{15}N, ^{17}O, and ^{19}F) and 3.48/3.23 (total) ppm with respect to the experimental shifts δ_0; and MADs of 2.44/2.06 (^{13}C), 6.91/3.05 (^{15}N, ^{17}O, and ^{19}F) and 3.59/2.26 (total) ppm with respect to the experimental shifts (δ_e), when the pathological case of F_2 is excluded. These are comparable in accuracy with the MP2 results at the experimental geometries.[23,24] Such systematic error cancellation may lead to a pragmatic protocol as shown in ref. 67.

Conclusions

We perform a systematic examination on the dependence of the calculated nuclear magnetic shielding constants on the chosen geometry for a selective set of density functional methods of B3LYP, PBE0, and OPBE. The testing set includes the ^{13}C, ^{15}N, ^{17}O, and ^{19}F magnetic shieldings and chemical shifts of 23 molecules with 34 nuclei. The geometries used are the experimental geometries or the optimized geometries at the levels of HF, MP2, or B3LYP.

We find that the accuracy for the geometry prediction follows the order that MP2/L > B3LYP/L > B3LYP/S > MP2/S > HF/S > HF/L. The general trend is that increasing the basis set tends to decrease the bond lengths and increase the bond angles. Large basis set does not always guarantee a convergence to the experimental value due to the limitation of the method employed.

We conclude that the OPBE exchange-correlation functional performs remarkably well for the whole set of the testing system. At the experimental geometries, OPBE leads to the mean

absolute deviations (MADs) of 2.19 (for ^{13}C) and 6.97 ppm (for ^{15}N, ^{17}O, and ^{19}F), giving a total MAD of 3.88 ppm, with respect to the gas phase experimental shieldings (σ_0). The corresponding MADs for chemical shifts associated with OPBE, with respect to the experimental chemical shifts (δ_0) are 1.99 (^{13}C), 9.23 (^{15}N, ^{17}O, and ^{19}F) and 4.16 (total) ppm. This good performance stands when the optimized geometries are used or when the rovibrational effects are taken into account.

The popular B3LYP functional suffers from a severe shortcoming of deshielding, giving shieldings that are too low and shifts that are too high at the experimental geometries. PBE0 shows a similar tendency of deshielding, but to a less extent. Combined with the HF geometries, however, much improved magnetic constants are obtained for B3LYP and PBE0, due to the compensation effect from the systematic underestimation of bond lengths by the HF method. Thus B3LYP/PBE0 at the HF/6-31G(d) geometries lead to MADs of 5.65/1.99 (^{13}C), 5.64/5.03 (^{15}N, ^{17}O, and ^{19}F) and 5.64/3.00 (total) ppm with respect to the experimental shieldings (σ_0); and MADs of 2.36/2.12 (^{13}C), 6.69/6.42 (^{15}N, ^{17}O, and ^{19}F) and 3.48/3.23 (total) ppm with respect to the experimental shifts (δ_0), when the pathological case of F_2 is excluded.

References

1. Jameson, C. J. Annu Rev Phys Chem 1996, 47, 135.
2. Nakatsuji, H. J Chem Phys 1974, 61, 3728.
3. Koch, W.; Holthausen, M. C. A Chemist's Guide to Density Functional Theory; Wiley: New York, 2000.
4. Helgaker, T.; Jaszunski, M.; Ruud, K. Chem Rev 1999, 99, 293.
5. Gauss, J. J Chem Phys 1993, 99, 3629.
6. Kollwitz, M.; Gauss, J. Chem Phys Lett 1996, 260, 639.
7. Cybulski, S. M.; Bishop, D. M. J Chem Phys 1997, 106, 4082.
8. Gauss, J.; Stanton, J. F. J Chem Phys 1995, 103, 3561.
9. Gauss, J.; Stanton, J. F. J Chem Phys 1996, 104, 2574.
10. Christiansen, O.; Gauss, J.; Stanton, J. F. Chem Phys Lett 1997, 266, 53.
11. Hansen, A. E.; Bouman, T. D.In Nuclear Magnetic Shieldings and Molecular Structure; Tossell, J. A., Ed.; Kluwer: Dordrecht, The Netherlands, 1993; pp. 117–140.
12. Kutzelnigg, W.; van Wullen, C.; Fleischer, U.; Franke, R.; Mourik, T. V. In Nuclear Magnetic Shieldings and Molecular Structure; Tossell, J. A., Ed.; Kluwer: Dordrecht, The Netherlands, 1993; pp. 141–161.
13. van Wullen, C.; Kutzelnigg, W. J Chem Phys 1996, 104, 2330.
14. Wilson, P. J.; Amos, R. D.; Handy, N. C. Chem Phys Lett 1999, 312, 475.
15. Cheeseman, J. R.; Trucks, G. W.; Keith, T. A.; Frisch, M. J. J Chem Phys 1996, 104, 5497.
16. Adamo, C.; Barone, V. Chem Phys Lett 1998, 298, 113.
17. Magyarfalvi, G.; Pulay, P. J Chem Phys 2003, 119, 1350.
18. Patchkovskii, S.; Autschbach, J.; Ziegler, T. J Chem Phys 2001, 115, 26.
19. Malkin, V. G.; Malkina, O. L.; Casida, M. E.; Salahub, D. R. J Am Chem Soc 1994, 116, 5898.
20. Lee, A. M.; Handy, N. C.; Colwell, S. M. J Chem Phys 1995, 103, 10095.
21. Cohen, A. J.; Wu, Q.; Yang, W. Chem Phys Lett 2004, 399, 84.
22. Keal, T. W.; Tozer, D. J.; Helgaker, T. Chem Phys Lett 2004, 391, 374.
23. Zhang, Y.; Wu, A.; Xu X.; Yan, Y. J. Chem Phys Lett 2006, 421, 383.
24. Wu, A.; Zhang, Y.; Xu, X.; Yan, Y. J. J Comput Chem 2007, 28, 2431.
25. Becke, A. D. J Chem Phys 1993, 98, 5648.
26. Slater, J. C. Quantum Theory of Molecules and Solids, Vol. 4: The Self-Consistent Field for Molecules and Solids; McGraw Hill: New York, 1974.
27. Becke, A. D. Phys Rev B 1988, 38, 3098.
28. Vosco, S. H.; Wilk, L.; Nusiair, M. Can J Phys 1980, 58, 1200.
29. Lee, C.; Yang, W.; Parr, R. G. Phys Rev B 1988, 37, 785.
30. Adamo, C.; Barone, V. Chem Phys Lett 1998, 298, 113.
31. Perdew, J. P.; Burke, K.; Ernzerhof, M. Phys Rev Lett 1996, 77, 3865.
32. Perdew, J. P.; Ernzerhof, M. J Chem Phys 1996, 105, 9982.
33. Cohen, A. J.; Handy, N. C. Chem Phys Lett 2000, 316, 160.
34. Jameson, A. K.; Jameson, C. J. Chem Phys Lett 1987, 134, 461.
35. Jameson, C. J.; Jameson, A. K.; Oppusungu, D.; Wille, S.; Burrell, P. M. J Chem Phys 1981, 74, 81.
36. Wasylishen, R. E.; Bryce, D. L. J Chem Phys 2002, 117, 10061.
37. Makulski, W.; Jackowski, K. Chem Phys Lett 2001, 341, 369.
38. Jameson, C. J.; Jameson, A. K.; Burrell, P. M. J Chem Phys 1980, 73, 6013.
39. Hindermann, D. K.; Cornwell, C. D. J Chem Phys 1968, 48, 4142.
40. Fowler, P. W.; Raynes, W. T. Mol Phys 1981, 43, 65.
41. Jameson, C. J.; de Dios, A. C.; Jameson, A. K. J Chem Phys 1991, 95, 1069.
42. Raynes, W. T.; Fowler, P. W.; Lazzeretti, P.; Zanasi, R.; Grayson, M. Mol Phys 1988, 64, 143.
43. Paidarova, I.; Komasa, J.; Oddershede, J. Mol Phys 1991, 72, 559.
44. Jameson, C. J.; Jameson, A. K.; Wille, S.; Burrell, P. M. J Chem Phys 1981, 74, 853.
45. Jameson, C. J.; Jameson, A. K.; Burrell, P. M. J Chem Phys 1980, 73, 6013.
46. Auer, A. A.; Gauss, J.; Stanton, J. F. J Chem Phys 2003, 118, 10407.
47. Åstrand, P.-O.; Ruud, K. Phys Chem Chem Phys 2003, 5, 5015.
48. Ruud, K.; Åstrand, P.-O.; Taylor, P. R. J Am Chem Soc 2001, 123, 4826.
49. Ditchfield, R. J Chem Phys 1972, 56, 5688.
50. Frisch, M. J.; Trucks, G. W.; Schlegel, H. B.; Scuseria, G. E.; Robb, M. A.; Cheeseman, J. R.; Montgomery, J. A., Jr.; Vreven, T.; Kudin, K. N.; Burant, J. C.; Millam, J. M.; Iyengar, S. S.; Tomasi, J.; Barone, V.; Mennucci, B.; Cossi, M.; Scalmani, G.; Rega, N.; Petersson, G. A.; Nakatsuji, H.; Hada, M.; Ehara, M.; Toyota, K.; Fukuda, R.; Hasegawa, J.; Ishida, M.; Nakajima, T.; Honda, Y.; Kitao, O.; Nakai, H.; Klene, M.; Li, X.; Knox, J. E.; Hratchian, H. P. Cross, J. B.; Adamo, C.; Jaramillo, J.; Gomperts, R.; Stratmann, R. E.; Yazyev, O.; Austin, A. J.; Cammi, R.; Pomelli, C.; Ochterski, J. W.; Ayala, P. Y.; Morokuma, K.; Voth, G. A.; Salvador, P.; Dannenberg, J. J.; Zakrzewski, V. G.; Dapprich, S.; Daniels, A. D.; Strain, M. C.; Farkas, O.; Malick, D. K.; Rabuck, A. D.; Raghavachari, K.; Foresman, J. B.; Ortiz, J. V.; Cui, Q.; Baboul, A. G.; Clifford, S.; Cioslowski, J.; Stefanov, B. B.; Liu, G.; Liashenko, A.; Piskorz, P.; Komaromi, I.; Martin, R. L.; Fox, D. J.; Keith, T.; Allaham, M. A.; Peng, C. Y.; Nanayakkara, A.; Challacombe, M.; Gill, M. W.; Johnson, B.; Chen, W.; Wong, M. W.; Gonzalez, C.; People, J. A. Gaussian 03; Gaussian: Wallingford, CT, 2004.
51. Bak, K. L.; Gauss, J.; Jørgensen, P.; Olsen, J.; Helgaker, T.; Stanton, J. F. J Chem Phys 2001, 114, 6548.
52. Callonion, J. H.; Hirota, E.; Kuchitsu, K.; Lafferty, W. J.; Maki, A. G.; Pote, C. S. In Landolt-Bornstein: Numerical Data and Function Relationships in Science and Technology; Hellwege, K. H., Ed.;

Springer-Verlag: West Berlin, 1976; Vol. 7. New Series: Structure Data on Free Polyatomic Molecules.
53. Huber, K. P.; Herzberg, G. H. Molecular Spectra and Molecular Structure. IV. Constants of Diatomic Molecules; Van Nostrand-Reinhold: New York, 1979.
54. Landolt-Bornstein.New Series: Structure Data of Free Polyatomic Molecules, Vol. 23:Numerical Data and Function Relationships in Science and Technology; Kuchitsu, K., Ed.; Springer-Verlag: West Berlin, 1995.
55. Bartell, L. S.; Kuchitsu, K.; deNeui, R. J. J Chem Phys 1961, 35, 1211.
56. Spiridonov, V. P.; Vogt, N.; Vogt, J. Struct Chem 2001, 12, 349.
57. Ohshima, Y.; Yamamoto, S.; Nakata, M.; Kuchitsu, K. J Phys Chem 1987, 91, 4696.
58. Brodersen, S. J Mol Spectrosc 1991, 145, 331.
59. Le Guennec, M.; Wlodarczak, G.; Burie, J.; Demaison, J. J Mol Spectrosc 1992, 154, 305.
60. Gerry, M. C. L.; Lees, R. M.; Winnewisser, G. J Mol Spectrosc 1976, 61, 231.
61. Ghosh, S. N.; Trambarulo, R.; Gordy, W. J Chem Phys 1952, 20, 605.
62. Cramer, G.; Rosetti, C.; Baily, D. Mol Phys 1986, 58, 627.
63. Margulès, L.; Demaison, J.; Boggs, J. E. Struct Chem 2000, 11, 145.
64. Curtiss, L. A.; Raghavachari, K.; Pople, J. A. J Chem Phys 1993, 98, 1293.
65. Bauschlicher, C. W. Jr.; Partridge, H. J Chem Phys 1995, 103, 1788.
66. Johnson, B. G.; Gill, P. M.W.; Pople, J. A. J Chem Phys 1993, 98, 5612.
67. Zhang, Y.; Wu, A.; Xu, X.; Yan, Y. J. J Phys Chem A 2007, 111, 9431.